International Journal of Multiphase Flow 35 (2009) 1149–1158

Contents lists available at ScienceDirect

International Journal of Multiphase Flow

journal homepage: www.elsevier.com/locate/ijmulflow

Mixing of miscible liquids in gas-segmented serpentine channels

Hakan Dogan [a], Selman Nas [b], Metin Muradoglu [a,*]

[a] Department of Mechanical Engineering, Koc University, Rumelifeneri Yolu, Sariyer, 34450 Istanbul, Turkey
[b] Department of Astronautical Engineering, Istanbul Technical University, Maslak, Istanbul, Turkey

ARTICLE INFO

Article history:
Received 6 March 2009
Received in revised form 6 July 2009
Accepted 16 July 2009
Available online 22 July 2009

Keywords:
Segmented gas-liquid flow
Chaotic mixing
Microfluidics
Finite-volume/front-tracking method

ABSTRACT

The chaotic mixing of miscible liquids in gas-segmented serpentine channels is studied computationally in a two-dimensional setting. Passive tracer particles are used to visualize and quantify the mixing. The molecular diffusion is ignored and only the mixing due to chaotic stirring is considered. Mixing is quantified using the entropy and intensity of segregation measures. The effects of various non-dimensional parameters on the quality of mixing are investigated and it is found that the relative bubble size, the capillary number and the non-dimensional channel corrugation length are the most important parameters influencing the mixing. The mixing is found to be weakly dependent on Reynolds number and nearly independent of viscosity ratio.

1. Introduction

Rapid mixing of fluids in microchannels is an important but challenging problem in modern engineering applications such as nanoparticle synthesis, enzyme reactions, drug delivery, DNA analysis and protein folding (Shui et al., 2007; Stone et al., 2004). The flows are usually highly laminar and thus mixing is notoriously difficult in such channels. Due to absence of turbulence, the mixing mainly relies on molecular diffusion that is usually insufficient to mix fluids across the channel on the time scale of the usual residence time. Mixing is especially difficult for solutions containing large molecules that have lower diffusion coefficients than those of ordinary small molecules (Stone et al., 2004). Therefore mixing enhancement has become an important research area and a number of active and passive enhancement techniques have been developed for this purpose. Nearly all the mixing enhancement methods are based on the concept of chaotic stirring of miscible fluids (Aref, 1984). External actuation methods such as electrocapillary, termocapillary and acoustic actuation are examples of the active mixing methods (Stone et al., 2004) whereas settling multiphase flows (Garstecki et al., 2005; Gunther et al., 2005) and using patterned channel walls (Kang et al., 2007) are ways of passive enhancement. Here we computationally study the chaotic mixing in liquid slugs moving through gas-segmented serpentine channels drawing inspiration from the microfluidic devices developed by the Jensen's group for chemical synthesis (Guenther et al., 2004; Gunther et al., 2005; Khan et al., 2004; Yen et al., 2005) and biofluidic applications (El-Ali et al., 2005). The micromixer developed by Garstecki et al. (2005, 2006) also utilizes the gas bubbles to cause chaotic mixing in the host liquid but its working principle is based on the additional pressure drop caused by the existence of the gas bubble. The two-dimensional model serpentine channel used in the present study is shown in Fig. 1.

The inserted gas phase segments the liquid into small, isolated slugs and acts as a barrier between them due to the gas–liquid interfacial tension. The insertion of bubbles creates recirculation within the liquid slugs and induces additional pressure drop in the channel. In the case of a straight channel, there are two symmetrical and counter rotating steady vortices within the liquid slug in the reference frame moving with the centroid of the slug. Therefore there is no cross mixing in straight channel in the absence of molecular diffusion as discussed by Yu et al. (2007). However, this vortex symmetry is broken in the case of the curved channel. That is, the vortex at the top is larger than the vortex at the bottom when the channel is concave down and it is reversed when the channel is concave up. In the case of a serpentine channel, the large and small vortices switch positions periodically as the bubbles move through the channel as sketched in Fig. 2. This is the underlying physical mechanism causing chaotic stirring in the gas-segmented microchannels (Guenther et al., 2004; Gunther et al., 2005). The segmentation of the channel reduces axial dispersion significantly and only dispersion occurs due to either convection through liquid film between channel wall and gaseous phase or diffusion through the gas–liquid interface. In addition, the temporal variation of pressure distribution induced by the bubbles leads to stretching and folding of the continuous fluid in segmented flow (Garstecki et al., 2005). Hence the usage of immiscible phases reduces the axial dispersion and enhances the chaotic mixing

* Corresponding author. Tel.: +90 212 338 14 73; fax: +90 212 338 15 48.
E-mail addresses: hakdogan@ku.edu.tr (H. Dogan), nas@itu.edu.tr (S. Nas), mmuradoglu@ku.edu.tr (M. Muradoglu).

0301-9322/$ - see front matter © 2009 Elsevier Ltd. All rights reserved.
doi:10.1016/j.ijmultiphaseflow.2009.07.006

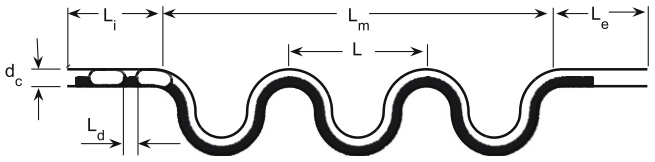

Fig. 1. The sketch of the model serpentine channel. The volume flow rate per unit width into the page is specified at the inlet based on a fully developed channel flow and the pressure is fixed at the exit. The flow is initialized as a single-phase steady flow using the ambient fluid properties and cylindrical bubbles are then placed instantaneously in the ambient flow. The tracer particles are initially distributed uniformly outside the bubbles at random and the particles filling the lower part of the channel are used for visualization.

(Yen et al., 2005). Gas–liquid segmentation is preferable to single-phase flow due to enhanced mixing and narrower residence time distributions (Yen et al., 2005). Also, it has advantages over liquid–liquid segmentation due to (i) having larger range of reaction time scales, (ii) easier methods of separation of phases after mixing and (iii) wider range of reaction temperature (Yen et al., 2005).

The chaotic streamline patterns in Stokes flows have been subject of a wide range of theoretical study in various geometries such as annular wedge (Krasnopolskaya et al., 1999), rectangular (Gaskell et al., 1998) and cylindrical (Meleshko et al., 2000) cavities. Similar studies have been also carried out for two-phase flows including liquid–liquid and gas–liquid systems (Bajer and Moffat, 1990; Kroujiline and Stone, 1999; Stone et al., 1991). The acquisition in this area yields to find out details of chaotic mixing inside droplets (Stone and Stone, 2005). Song et al. (2003) have shown that the reagents in a droplet can be mixed rapidly as the liquid drop moves through a winding channel. Muradoglu and Stone (2005) have investigated the chaotic mixing in a drop and studied the effects of capillary number, viscosity ratio, relative drop size and channel curvature. In this paper, we computationally investigate the chaotic mixing within liquid slugs segmented by an immiscible gaseous phase in curved channels using a similar computational setting employed by Muradoglu and Stone (2005) for studying chaotic mixing in viscous droplets.

The model winding channel used in this study consists of cocentric circular arcs connected sequentially to form three periods as sketched in Fig. 1. In the reference frame moving with the centroid of the liquid slug, the velocities at the inner and outer wall can be approximated in the limit of a vanishing capillary number by $V_{\text{top}} = 2(1+\beta)V_b/(2+\beta)$ and $V_{\text{bottom}} = 2V_b/(2+\beta)$, respectively (Muradoglu and Stone, 2007). Here V_b is the steady bubble velocity and $\beta = d_c/R_i$ is the non-dimensional curvature of the inner wall with d_c being the channel width, R_i the radius of the curvature of inner channel wall. As a result, the flow in the slug resembles a double-lid-driven cavity flow as sketched in Fig. 2. This analogy also indicates that the difference between the lid velocities and thus the mixing within the liquid slug increases with increasing channel curvature. In the case of a serpentine channel, the top and bottom lid velocities alternate periodically inducing unsteady and chaotic flow within the liquid slug and thus leading to rapid mixing of the solutions (Ottino, 1989). Gaskell et al. (1998) obtained an eigenfunction expansion solution of streamlines in a double-lid-driven cavity flow with free-surface side walls within a rectangular domain. When the lid velocities alternate time-periodically, the physical problem studied by Gaskell et al. (1998) becomes analogous to our problem but still not one to one correspondence since interactions between gas phase and liquid slug are not linear in the present problem. Therefore a model built on the Gaskell's solution would yield no dispersion between following liquid slugs as they are fully blocked by rectangular shaped bubbles in the channel. In addition these no-shear walls get closer in the segmented flow near the centerline of the winding channel, so the fluid volume near the middle of liquid slug is pushed towards the moving lids and thus recirculation is strengthened. Note that the secondary flow occurs in the three-dimensional meandering square channels and induces transverse recirculation in addition to longtitudinal recirculation. This transverse recirculation enhances mixing and thus heat and mass transfer in a microchannel as studied by Ahn et al. (2008).

In the present study, the mixing within the liquid slugs moving through a gas-segmented winding channel is studied computationally using the finite-volume/front-tracking (FV/FT) method developed by Muradoglu and Kayaalp (2006) in a simple two-dimensional setting in order to facilitate extensive numerical simulations. The molecular mixing is ignored and only mixing due to chaotic advection is considered. The mixing is visualized with passive tracer particles and is quantified in the same way as done by Muradoglu and Stone (2005). The effects of the relevant non-dimensional parameters such as the capillary number, Reynolds number, density and viscosity ratios and various geometrical

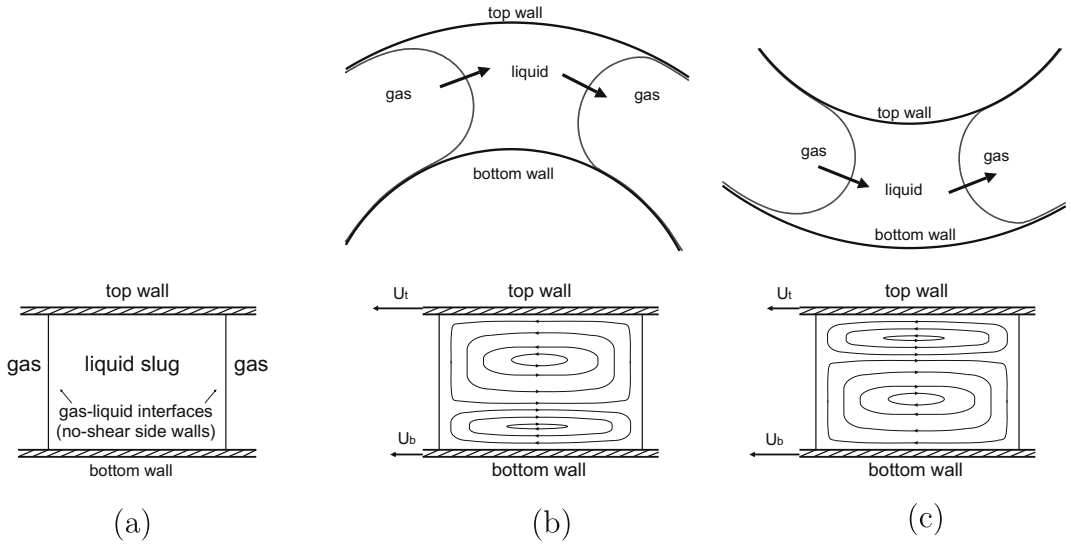

Fig. 2. The liquid slug between gas bubbles moving through curved channel resembles a lid-driven cavity flow in the limit of vanishing capillary number. The flow can be treated as if the slug is stationary and the top and bottom channel walls are moving. (a) Sketch for the lid-driven cavity flow. Concave up (b) and concave down (c) portions of the serpentine channel (top) and representative sketches for the corresponding lid-driven cavity flows (bottom).

parameters related to bubble size, slug length and channel corrugation wavelength are studied in details.

The organization of this paper is as follows: in Section 2, the mathematical formulation and computational method are discussed briefly. The physical problem is described and the techniques used for visualization and quantification of mixing are explained in Section 3. The results are presented and discussed in Section 4 and concluding remarks are summarized in Section 5.

2. Formulation and numerical method

The governing equations are described in this section in the form suitable for the front-tracking method. This method is based on a single-field formulation of flow equations for the entire computational domain and different phases are treated as a single Newtonian fluid with variable material properties (Tryggvason et al., 2001; Unverdi and Tryggvason, 1992). The effects of surface tension are treated as body forces and added to the momentum equations as δ functions at the phase boundaries. Following Muradoglu and Gokaltun (2004) and Muradoglu and Kayaalp (2006), the two-dimensional incompressible continuity and Navier–Stokes equations can be written in conservation form as

$$\frac{\partial \mathbf{q}}{\partial t}+\frac{\partial \mathbf{f}}{\partial x}+\frac{\partial \mathbf{g}}{\partial y}=\frac{\partial \mathbf{f}_v}{\partial x}+\frac{\partial \mathbf{g}_v}{\partial y}+\mathbf{f}_b, \tag{1}$$

where

$$\mathbf{q}=\begin{Bmatrix}0\\ \rho u\\ \rho v\end{Bmatrix},\quad \mathbf{f}=\begin{Bmatrix}u\\ \rho u^2+p\\ \rho uv\end{Bmatrix},\quad \mathbf{g}=\begin{Bmatrix}v\\ \rho uv\\ \rho v^2+p\end{Bmatrix}, \tag{2}$$

and

$$\mathbf{f}_v=\begin{Bmatrix}0\\ \tau_{xx}\\ \tau_{xy}\end{Bmatrix},\quad \mathbf{g}_v=\begin{Bmatrix}0\\ \tau_{xy}\\ \tau_{yy}\end{Bmatrix}. \tag{3}$$

In Eqs. (1)–(3), x and y are the Cartesian coordinates and t is the physical time; ρ, μ and p are the fluid density, the dynamic viscosity and pressure, respectively; and u and v are the velocity components in x and y coordinate directions, respectively. The first row in Eq. (1) simply states that the velocity field is solenoidal while the last two rows represent the momentum conservation equations in x and y directions, respectively. The viscous stresses appearing in the viscous flux vectors are given by

$$\tau_{xx}=2\mu\frac{\partial u}{\partial x},\quad \tau_{yy}=2\mu\frac{\partial v}{\partial y},\quad \tau_{xy}=\mu\left(\frac{\partial u}{\partial y}+\frac{\partial v}{\partial x}\right). \tag{4}$$

The last term in Eq. (1) represents the body forces resulting from surface tension and is given by

$$\mathbf{f}_b=\int_S \sigma\kappa\mathbf{n}\delta(\mathbf{x}-\mathbf{x}^f)ds, \tag{5}$$

where $\delta, \mathbf{x}^f, \sigma, \kappa$ and $\mathbf{n}$ denote, respectively, the Dirac delta function, the location of the interface, the surface tension coefficient, twice the mean curvature, the outward unit normal vector on the interface, and the integral is taken over the surface area of the interface, S.

In Eq. (1), it is assumed that the density and viscosity of a fluid particle remain constant, i.e.,

$$\frac{D\rho}{Dt}=0;\quad \frac{D\mu}{Dt}=0, \tag{6}$$

where the substantial derivative is defined as $\frac{D}{Dt}=\frac{\partial}{\partial t}+\mathbf{u}\cdot\nabla$.

The governing equations (Eq. (1)) are solved by the finite-volume/front-tracking method developed by Muradoglu and Kayaalp (2006). The method combines a finite-volume solver with the front-tracking method developed by Unverdi and Tryggvason (1992). The continuity and momentum equations are solved on a curvilinear grid using a finite-volume method. The spatial derivatives are approximated by a finite-volume method that is equivalent to second-order finite differences on a regular mesh. A dual (or pseudo) time-stepping method is employed to achieve time accuracy and an alternating direction implicit (ADI) method is used to perform integration in pseudo time. Fourth-order numerical dissipation terms are added to the discrete version of the flow equations to prevent the odd–even decoupling. Preconditioning, local time-stepping, and multigrid methods are used to accelerate the convergence rate of the ADI method in the pseudo time. Details of the FV method can be found in references (Muradoglu and Kayaalp, 2006; Caughey, 2001).

The interface boundary between the bubble and the ambient fluid are represented by connected Lagrangian marker points moving with the local flow velocity interpolated from the neighboring curvilinear grid nodes. The communication between the curvilinear grid and the interface marker points is maintained efficiently using an auxiliary regular Cartesian grid cast on the curvilinear grid (Muradoglu and Kayaalp, 2006). An indicator function is defined such that it is unity inside the bubbles and zero outside. Based on the locations of the interface marker points, unit magnitude jumps are distributed in a conservative manner on the regular grid points near the interface and are integrated to compute the indicator function everywhere. This procedure involves solution of a Poisson equation on a regular grid and yields a smooth transition of the indicator function across the interface. The indicator function is then interpolated from the regular Cartesian grid onto the curvilinear grid using bilinear interpolations. Once the indicator function distribution is determined, the viscosity and density are set as a function of the indicator function. The interface marker points are also used to compute the surface tension forces at the interface which are then distributed on the neighboring curvilinear grid cells in a conservative manner and added to the discrete momentum equations as source terms. The numerical method is essentially the same as that used by Muradoglu and Stone (2005), and the readers are referred to Muradoglu and Kayaalp (2006) and Muradoglu and Gokaltun (2004) for the details.

3. Problem statement and quantification of mixing

3.1. Problem statement

The chaotic mixing within a liquid slug moving through a gas-segmented serpentine channel is studied in a two-dimensional setting. The model channel consists of a straight entrance, a curved mixer of three periods and a straight exit section as sketched in Fig. 1. The curved section of the mixer consists of cocentric circular arcs, the inner circle of a half period connects tangentially with the outer circle of the next half period. As discussed before, the flow field within the liquid slug moving through a curved channel resembles a double-lid-driven cavity flow with free-surface side walls (gas–liquid interface) and recirculation occurs due to motion of the walls and segmentation of liquid. The ratio of lid velocities is dependent on the channel curvature and thus the lid velocities switch when the channel curvature changes. Consequently, streamline patterns are antisymmetric with respect to centerline (see Fig. 2) and they cross each other over half periods, thus flow is time-dependent. The non-dimensional parameter $\kappa=d_c/L$ is used to characterize the geometry. The smaller the values of κ the weaker is the winding of the mixing section. The flow rate is specified at the inlet of the channel assuming a fully developed velocity profile with an average flow velocity of V_c. A steady

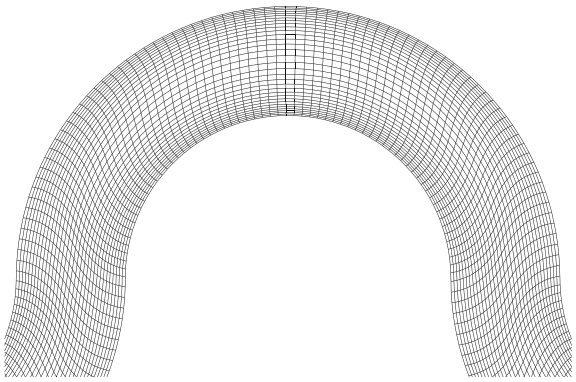

Fig. 3. A portion of a typical computational (coarse) grid containing 864×32 cells. Computations are performed on finer versions of this grid, e.g., containing 1728×64 cells.

single-phase flow is computed first using the ambient fluid (liquid) properties and is then used as the initial conditions. The bubbles are instantaneously placed in the channel close to the inlet. The bubble size is specified much larger than the channel width and are initialized with an approximate steady shape consisting of a straight middle and a semicircular back and front sections. The properties of the bubble phase and ambient fluid are denoted by subscripts "*i*" and "*o*", respectively. The governing non-dimensional parameters are defined as the channel Reynolds number $Re = \rho_o V_c d_c/\mu_o$, the capillary number $Ca = \mu_o V_c/\sigma$, the viscosity ratio $\lambda = \mu_i/\mu_o$, the density ratio $r = \rho_i/\rho_o$, the ratio of initial distance between bubbles to the channel width at the inlet $\eta = L_d/d_c$ and the ratio of the equivalent bubble diameter (d_b) to the channel width $\Lambda = d_b/d_c$. Based on the inlet velocity and the corrugation wave length, the non-dimensional physical time is defined as $t^* = tV_c/L$.

Passive tracer particles are initially distributed uniformly at random in the channel outside of the bubbles and the particles occupying the lower half of the channel are identified as "red" while the other particles are "blue". Note that only the particles that initially occupy the lower half of the channel are used in all the scatter plots presented in this paper. The tracer particles are

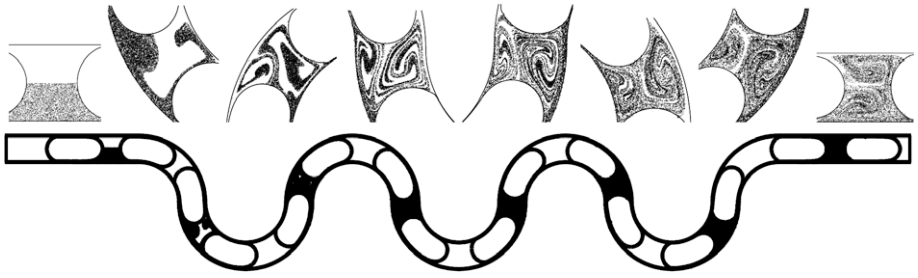

Fig. 4. Snapshots of mixing patterns for a two-bubble system taken at the non-dimensional times from left to right $t^* = 0, 5, 11, 16, 21.5, 27, 32.5$ and 38.5, respectively. The top plots are the enlarged versions of the corresponding scatter plots shown in the channel (lower plots). ($Ca = 0.005, Re = 0.64, \lambda = 0.014, \Lambda = 2.0, \eta = 0.75, \kappa = 0.125, r = 0.1$, grid: 1728×64.)

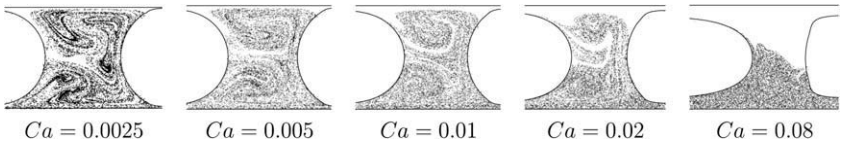

Fig. 5. Effects of capillary number (Ca) on mixing. The mixing patterns at the exit of the channel. ($Re = 0.64, \lambda = 0.014, \Lambda = 2.0, \eta = 0.75, \kappa = 0.125, r = 0.1$, grid: 1728×64.)

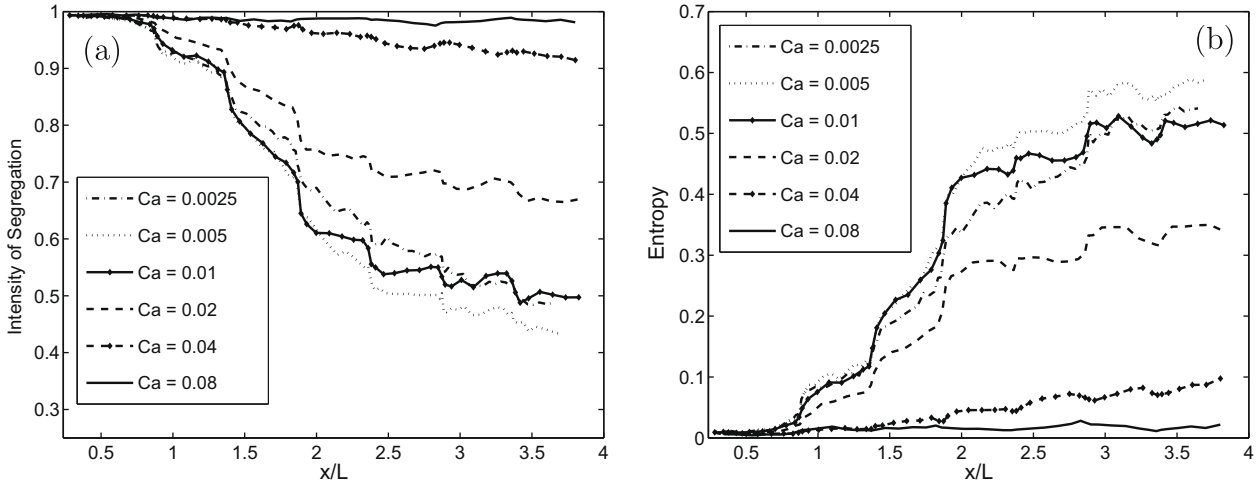

Fig. 6. Effects of the capillary number on mixing. (a) Intensity of segregation (b) entropy. ($Re = 0.64, \lambda = 0.014, \Lambda = 2.0, \eta = 0.75, \kappa = 0.125, r = 0.1$, grid: 1728×64.)

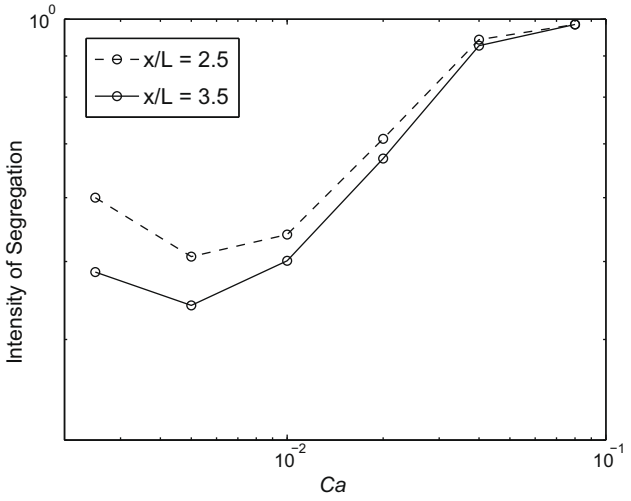

Fig. 7. The intensity of segregation against the capillary number at times when slug centroid, $x/L = 2.5$ and $x/L = 3.5$. The best mixing occurs at about $Ca = 0.005$. ($Re = 0.64, \lambda = 0.014, \Lambda = 2.0, \eta = 0.75, \kappa = 0.125, r = 0.1$, grid: 1728×64.)

introduced into channel when the bubbles take their steady shapes in the inlet section of the channel. The particles are moved with the local flow velocity interpolated from the neighboring computational grid points using the same advection scheme as used for moving the interface marker points.

Finally we complete the specification of the geometry by fixing L_i, the length of the inlet portion of the channel, L_e, the length of the exit portion of the channel, and L_m, the length of the mixing portion of the channel as sketched in Fig. 1.

3.2. Quantification of mixing

The mixing is visualized and quantified in a similar way as done by Muradoglu and Stone (2005). The tracer particles are used to visualize the mixing patterns within the liquid slugs and entropy and intensity of segregation measures are used to quantify the quality of mixing (Krasnopolskaya et al., 1999; Muradoglu and Stone, 2005). For this purpose, the liquid slug area S_s is divided into N_δ square pixels of width size δ for a side with an area of $S_\delta = \delta^2$ so that the slug area can be written approximately as $S_s \cong N_\delta S_\delta$. Note that the slug area is defined as the area occupied by liquid between centroid of bubbles. Then a coarse-grained probability density function is defined as $D_n = \frac{N_b^{(n)}}{N_b^{(n)}+N_r^{(n)}}$, where $N_b^{(n)}$ and $N_r^{(n)}$ are the number of "blue" and "red" tracer particles in the n^{th} pixel, respectively. Based on the coarse-grained density, the entropy of the mixture is defined as

$$s = -\langle D \log D \rangle. \tag{7}$$

The entropy is always positive since $0 < D < 1$ and grows in time to its maximum

$$s_o = -\lim_{t\to\infty}\langle D \log D\rangle = -\langle D\rangle \log\langle D\rangle, \tag{8}$$

when the fluids in the slug are fully mixed. In all the results presented in this study, the entropy is normalized by s_o. Finally, the intensity of segregation is defined as

$$I = \frac{\langle (D - \langle D\rangle)^2\rangle}{\langle D\rangle(1-\langle D\rangle)}. \tag{9}$$

In the case of complete mixing, the intensity of segregation tends to zero since the quantity $\langle (D - \langle D\rangle)^2\rangle$ tends to zero. The quality of mixing denoted by Q can be defined as the inverse of the intensity

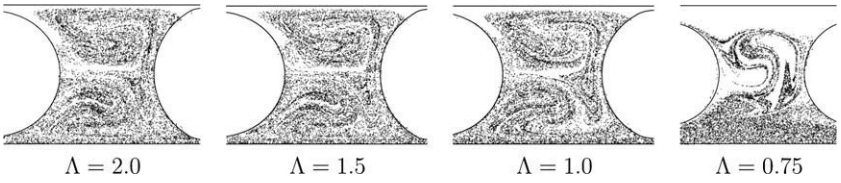

Fig. 8. Effects of the non-dimensional bubble size on the mixing. The mixing patterns at the exit of the channel for $\Lambda = 2.0, 1.5, 1.0$ and 0.75 from left to right, respectively. ($Ca = 0.005, Re = 0.64, \lambda = 0.014, \eta = 0.75, \kappa = 0.125, r = 0.1$, grid: 1728×64.)

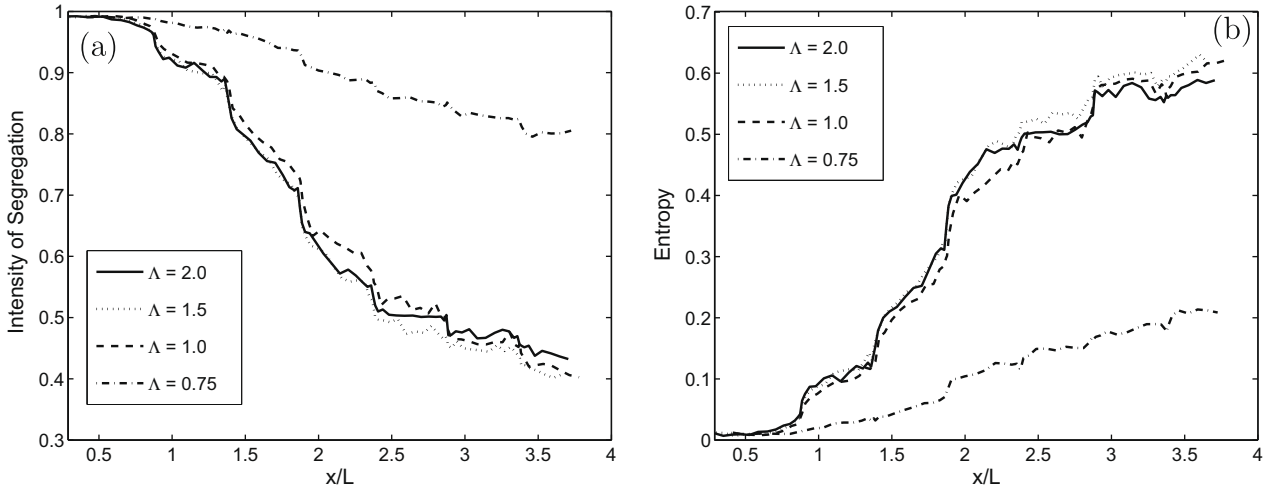

Fig. 9. Effect of bubble size on mixing. (a) Intensity of segregation (b) entropy. ($Ca = 0.005, Re = 0.64, \lambda = 0.014, \eta = 0.75, \kappa = 0.125, r = 0.1$, grid: 1728×64.)

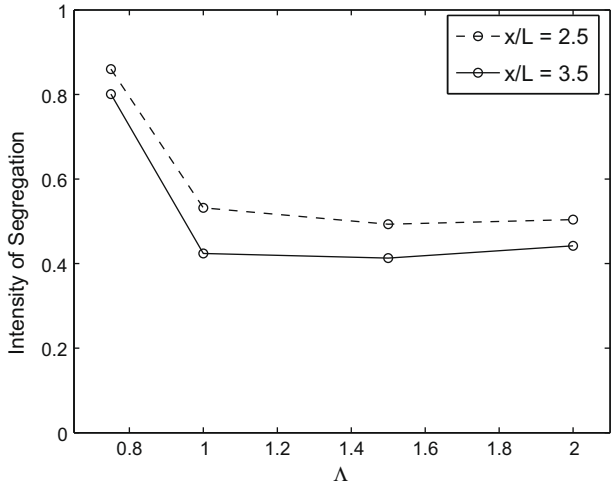

Fig. 10. The intensity of segregation against the non-dimensional bubble size at times when slug centroid, $x/L = 2.5$ and $x/L = 3.5$. The mixing is essentially independent of the bubble size when $\Lambda \geqslant 1$. ($Ca = 0.005, Re = 0.64, \lambda = 0.014, \eta = 0.75, \kappa = 0.125, r = 0.1$, grid: 1728×64.)

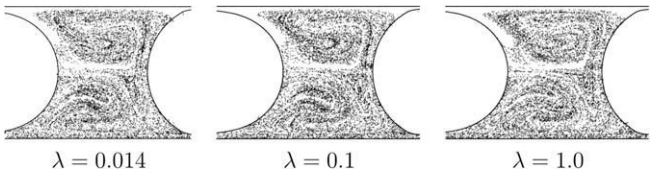

Fig. 11. Effects of viscosity ratio on the mixing. The mixing patterns at the exit of the channel for $\lambda = 0.014, 0.1$ and 1. ($Ca = 0.005, Re = 0.64, \Lambda = 2.0, \eta = 0.75, \kappa = 0.125, r = 0.1$, grid: 1728×64.)

of segregation, i.e., $Q = 1/I$. However, following Muradoglu and Stone (2005), the intensity of segregation is preferred in the present study over the mixing quality since it varies between zero and unity. Details of the entropy and segregation of intensity measures can be found in Krasnopolskaya et al. (1999), Muradoglu and Stone (2005).

4. Results and discussion

In this section, the computational results for mixing in liquid slugs between large bubbles moving through a serpentine channel are presented. The problem is studied in a two-dimensional setting in order to facilitate extensive numerical simulations. The overall structure of a typical (coarse) computational grid with 864×32 cells is shown in Fig. 3. Computations are performed on finer versions of this grid containing 1728×64 cells unless specified otherwise. The grid is stretched near the solid wall in order to resolve the liquid film between the bubble and the channel. A extensive grid convergence study is not repeated here since this grid resolution has been shown to be sufficient to obtain grid independent results for this kind of problems (Muradoglu and Stone, 2005, 2007; Muradoglu et al., 2007). The density ratio is kept constant at $r = 0.1$ in all the results presented here. Note that density has no significant effect in the low-Reynolds number flow as studied here.

First the evolution of mixing patterns in a liquid slug moving through the model serpentine channel is presented. Then the effects of the non-dimensional parameters such as the capillary number (Ca), the non-dimensional bubble size (Λ), the viscosity ratio (λ), the Reynolds number (Re), the relative initial distance between bubbles (η) and non-dimensional corrugation wavelength of the mixing section (κ) are examined. Scatter plots of the tracer particles are used to visualize the mixing patterns in the liquid slug and only the particles initially occupying the lower part of the channel are plotted in "black" for visual clarity. The particles crossing the bubble interface due to numerical error are reflected back into the liquid phase in the same was as done by Muradoglu et al. (2007). Some particles leak through the liquid film between the bubble and channel wall even in the absence of the molecular diffusion since the liquid film thickness changes periodically depending on the channel curvature as pointed out by Muradoglu and Stone (2007). The particles that leak through the liquid film are simply disregarded in the present results. In computing the intensity of segregation and entropy, the total number of tracer particles is initially set to 85,000 and the pixel size is determined such that there are about 10 particles in each pixel.

The snapshots of the tracer particles within the liquid slug are plotted in Fig. 4 at non-dimensional times of $t^* = 0, 5, 11, 16, 21.5, 27, 32.5$ and 38.5 to demonstrate the evolution of the mixing patterns as the slug moves through the model gas-segmented winding channel. The simulation is performed for the non-dimensional parameters of $Ca = 0.005, Re = 0.64, \Lambda = 2, \lambda = 0.014, \eta = 0.75, \kappa = 0.125$, and $r = 0.1$. This case is taken as the *base case* and the effects of the non-dimensional parameters are examined by systematically varying them one at a time. Note that typical values used in experiments (Gunther et al., 2005) are $\rho_o \simeq 789\ \mathrm{kg/m^3}, \rho_i \simeq 1.16\ \mathrm{kg/m^3}, \mu_o \simeq 1.19 \times 10^{-3}\ \mathrm{N\,s/m^2}, \mu_i \simeq$

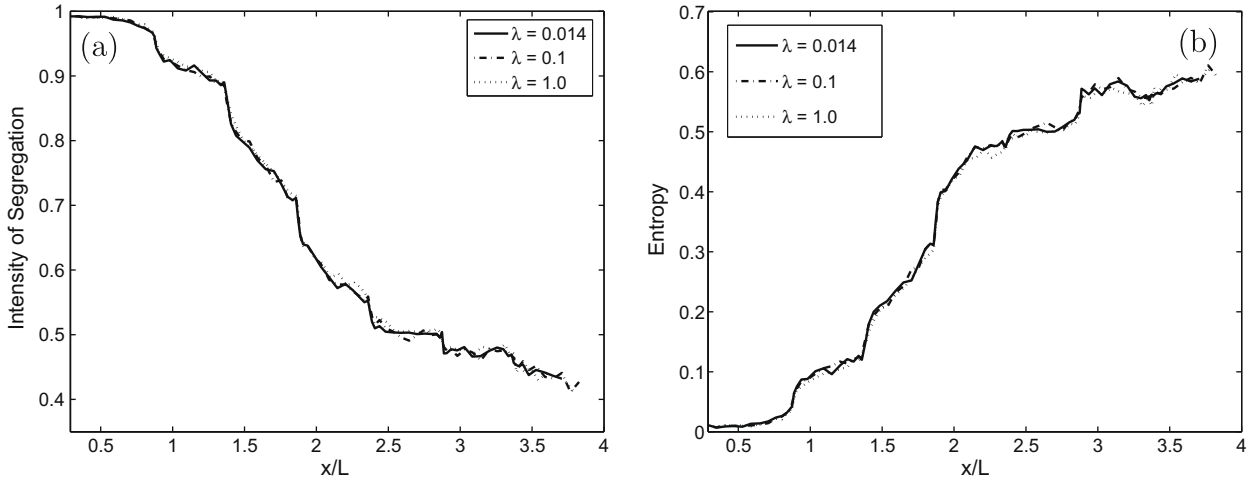

Fig. 12. Effect of the viscosity ratio on mixing. (a) Intensity of segregation (b) entropy. ($Ca = 0.005, Re = 0.64, \Lambda = 2.0, \eta = 0.75, \kappa = 0.125, r = 0.1$, grid: 1728×64.)

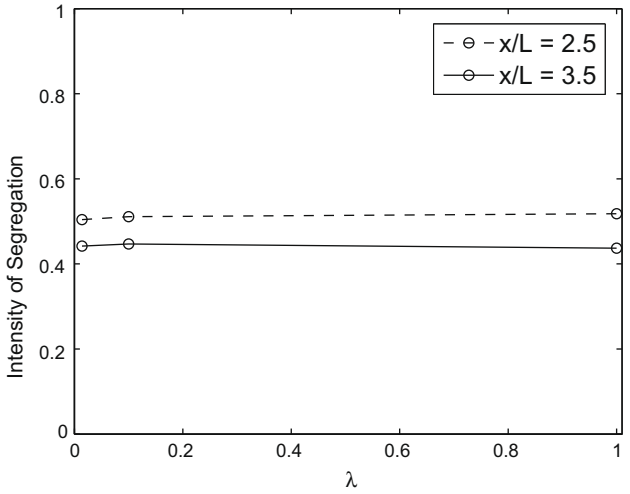

Fig. 13. The intensity of segregation against the viscosity ratio at times when slug centroid, $x/L = 2.5$ and $x/L = 3.5$. The mixing is nearly independent of the viscosity ratio, λ. ($Ca = 0.005, Re = 0.64, \Lambda = 2.0, \eta = 0.75, \kappa = 0.125, r = 0.1$, grid: 1728×64.)

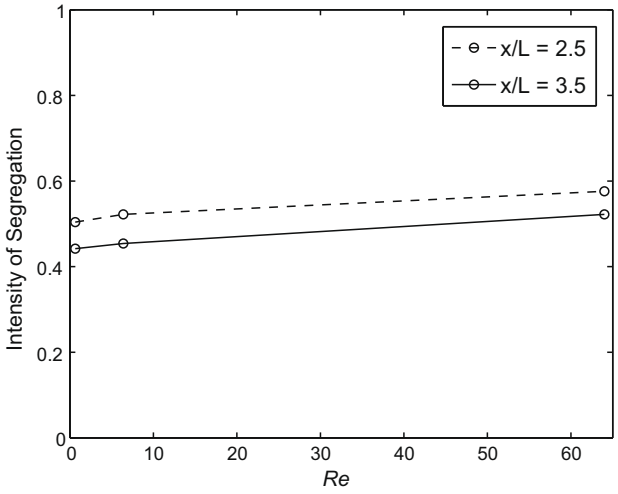

Fig. 16. The intensity of segregation against the Reynolds number at times when slug centroid, $x/L = 2.5$ and $x/L = 3.5$. The mixing slightly increases as the Re decreases. ($Ca = 0.005, \lambda = 0.014, \Lambda = 2.0, \eta = 0.75, \kappa = 0.125, r = 0.1$, grid: 1728×64.)

1.76×10^{-5} N s/m^2, $U_o \simeq 5.5$ mm/s, $d_c \simeq 22.4 \times 10^{-5}$ m and $\sigma \simeq 0.023$ N/m, which yields a Reynolds number approximately $Re \simeq 0.7$, a capillary number $Ca \simeq 0.0003$ and a viscosity ratio $\lambda \simeq 0.015$. We note that the present simulations are performed for larger capillary numbers than this typical experimental value due to numerical difficulty to resolve the liquid film between the gas bubble and the channel wall at very small capillary numbers. The liquid film thickness h_{liquid} scales as $h_{\text{liquid}}/d_c \sim Ca^{-2/3}$ (Bretherton, 1961; Muradoglu and Stone, 2007) and becomes extremely thin at small values of the capillary numbers. In addition, it is sufficient to keep the capillary number $Ca \leqslant 0.01$ to achieve segmentation and further decrease in the capillary number beyond this value does not affect the quality of mixing significantly as will be discussed below. The mixing patterns are enlarged in the top plots of Fig. 4 to better show the details of the mixing process. It is clear that chaotic advection occurs in a liquid slug as it moves through the winding channel.

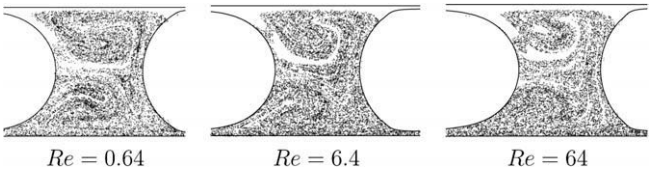

Fig. 14. Effects of Reynolds number on mixing. The mixing patterns at the exit of the channel for $Re = 0.64, 6.4$ and 64. ($Ca = 0.005, \lambda = 0.014, \Lambda = 2.0, \eta = 0.75, \kappa = 0.125, r = 0.1$, grid: 1728×64.)

We now present effects of the non-dimensional parameters on the quality of mixing. First the effects of the capillary number is examined. For this purpose, the mixing patterns are plotted in Fig. 5 at the exit of the channel for capillary numbers $Ca = 0.0025, 0.005, 0.01, 0.02$ and 0.08 while the other parameters are kept constant at the base values. As can be seen in this figure, the mixing increases as the capillary number is decreased. The effects of the capillary number are quantified in Fig. 6 where the intensity of segregation and entropy are plotted as a function of the non-dimensional x-component of the centroid of the liquid slug, x/L. The intensity of segregation is also plotted against Ca in Fig. 7 at times when $x/L = 2.5$ and $x/L = 3.5$. These figures show that the mixing is very poor for $Ca = 0.08$ and increases rapidly

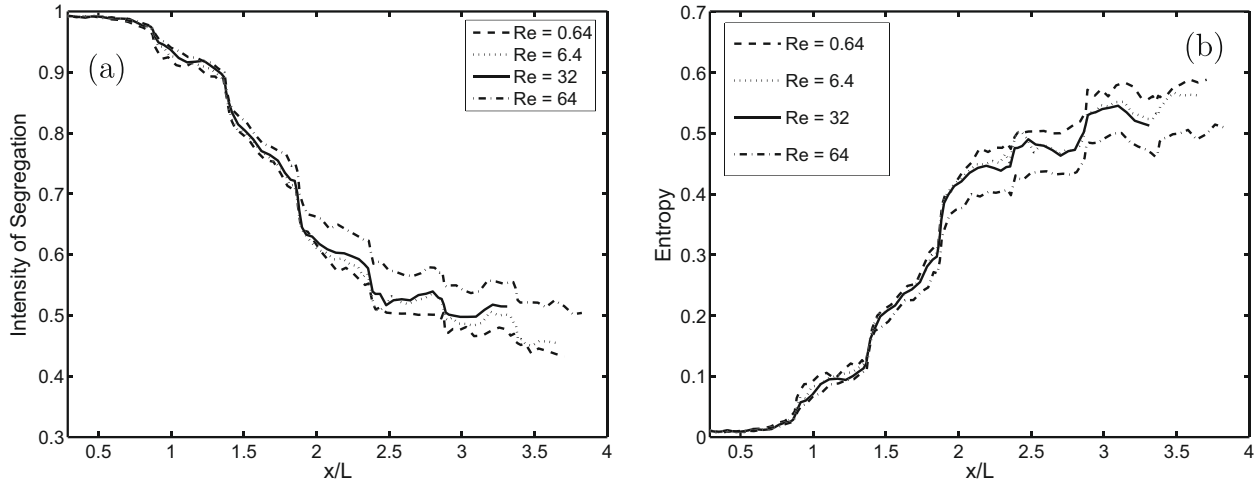

Fig. 15. Effect of the Reynolds number on mixing. (a) Intensity of segregation (b) entropy. ($Ca = 0.005, \lambda = 0.014, \Lambda = 2.0, \eta = 0.75, \kappa = 0.125, r = 0.1$, grid: 1728×64.)

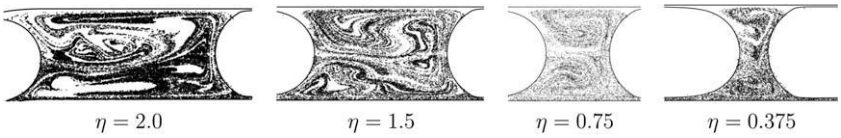

Fig. 17. The mixing patterns at the exit of the channel as a function of the initial distance between bubbles. ($Ca = 0.005, Re = 0.64, \lambda = 0.014, \Lambda = 2.0, \kappa = 0.125, r = 0.1$, grid: 1728×64.)

as Ca decreases until $Ca = 0.01$ but then the mixing is essentially unaffected by further decrease in the capillary number. For large capillary numbers, segmentation does not occur due to extreme deformability of the bubbles, and thus the mixing is poor. Once the segmentation occurs, the further decrease in capillary number does not improve the quality of mixing dramatically. It is also observed in Fig. 6 that each of the scalar measures such as the intensity of segregation and the entropy are consistent in representing the quality of mixing as also reported by Muradoglu and Stone (2005).

We next examine the effects of the relative bubble size on mixing. The non-dimensional bubble size is defined as the ratio of the equivalent diameter of the bubble to the channel width and its effects on the mixing are first presented in terms of the scatter plots in Fig. 8. The computations are performed for the relative bubble sizes of $\Lambda = 2.0, 1.5, 1.0$ and 0.75 while the other parameters are the same as those of the base case. The scatter plots are taken in the exit section of the channel, i.e., at $x/L = 3.5$. It is clearly seen from the figure that segmentation occurs when the bubble size is equal or larger than the channel width and the mixing quality is not sensitive to bubble size when $\Lambda \geqslant 1$. This is also verified by the intensity of segregation and entropy measures plotted in Fig. 9. The intensity of segregation is plotted against Λ in Fig. 10 at times when the non-dimensional component of slug centroid, $x/L = 2.5$ and $x/L = 3.5$. Figs. 5–10 indicate that the mixing quality is critically dependent on the segmentation and the chaotic advection occurs when the segmentation is achieved.

The effects of the viscosity ratio on the mixing are shown in Figs. 11–13. The mixing patterns in the exit section of the channel are plotted in Fig. 11 and the mixing is quantified in Fig. 12 for the viscosity ratios of $\lambda = 0.014, 0.1$, and 1.0. In addition, the intensity of segregation is plotted against λ in Fig. 13 at times when the non-dimensional component of slug centroid, $x/L = 2.5$ and $x/L = 3.5$. These figures indicate that the viscosity ratio is not a prime factor affecting the quality of mixing in liquid slugs as long as the segmentation is achieved. This is in contrast with the mixing inside a droplet moving through a serpentine channel where the viscosity ratio was found to be one of the main factors determining the quality of the mixing (Muradoglu and Stone, 2005).

The Reynolds number is typically small in flows in microchannels as studied here. Nevertheless the effects of the Reynolds number are examined here for completeness. For this purpose, Reynolds number is varied between $Re = 0.64$ and $Re = 64$ while the other parameters are set to the same values as used in the base case. Fig. 14 shows the mixing patterns in the exit section of the channel. This figure qualitatively illustrates that the quality of mixing is weakly dependent on the Reynolds number and mixing improves slightly as the Reynolds number increases. This observation is verified in Fig. 15 where the intensity of segregation and entropy are plotted as a function of x-component of the centroid of the liquid slug. In addition, the intensity of segregation is plotted against Re in Fig. 16 at times when $x/L = 2.5$ and $x/L = 3.5$. These figures clearly show that the quality of mixing increases slightly as the Reynolds number decreases. This result is consistent with the results obtained for the mixing in the droplet moving through a serpentine channel (Muradoglu and Stone, 2005).

Finally, we examine the effects of the geometric parameters on the quality of mixing in the liquid slugs. For this purpose, computations are performed for the various values of the relative distance between the bubbles ranging between $\eta = 2$ and $\eta = 0.375$ and the mixing patterns are plotted in Fig. 17. This figure shows that the best mixing is achieved about $\eta = 0.75$, i.e., in the base case. This observation is quantified and verified in Fig. 18 through the intensity of segregation and entropy measures and also in Fig. 19 where the intensity of segregation is plotted against η at times when $x/L = 2.5$ and $x/L = 3.5$. Recirculation within the liquid slug becomes weaker as η increases, thus some unmixed islands appear as can be seen, for instance, in Fig. 17 for $\eta = 2.0$. Another important geometric parameter is the corrugation wavelength of the channel normalized by the channel width. We finally present the

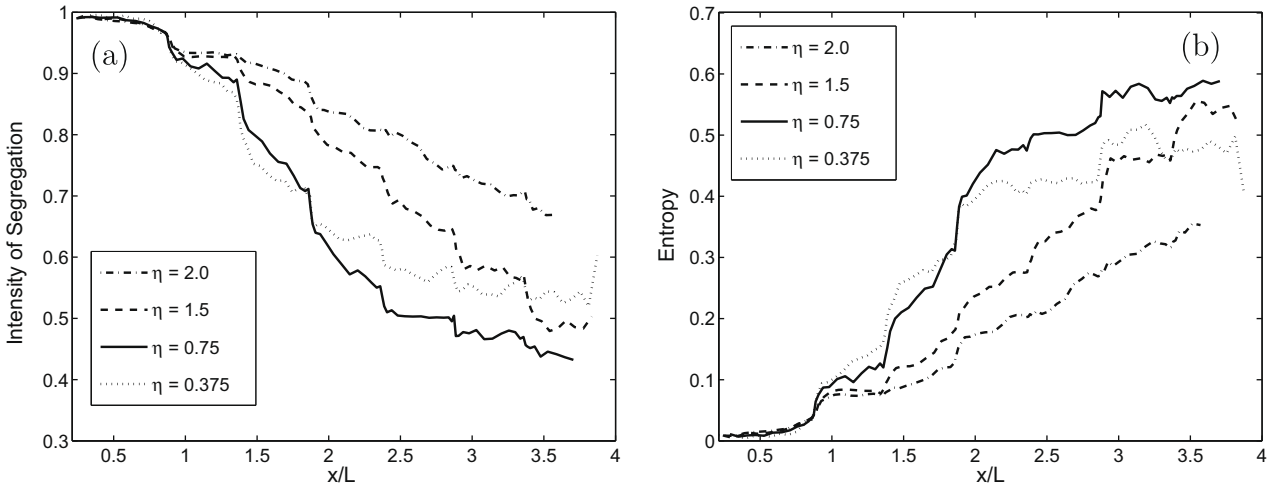

Fig. 18. Effect of the initial distance between bubbles on mixing. (a) Intensity of segregation (b) entropy. ($Ca = 0.005, Re = 0.64, \lambda = 0.014, \Lambda = 2.0, \kappa = 0.125, r = 0.1$, grid: 1728×64.)

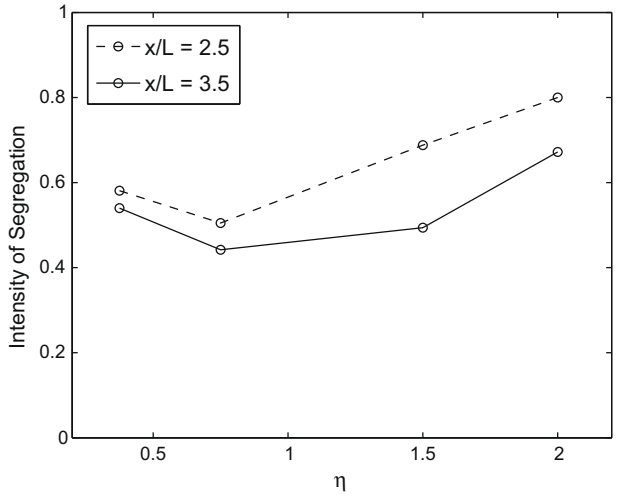

Fig. 19. The intensity of segregation against the non-dimensional distance between bubbles at times when slug centroid, $x/L = 2.5$ and $x/L = 3.5$. The best mixing occurs for the base case, i.e., $\eta = 0.75$. ($Ca = 0.005, Re = 0.64, \lambda = 0.014, \Lambda = 2.0, \kappa = 0.125, r = 0.1$, grid: 1728×64.)

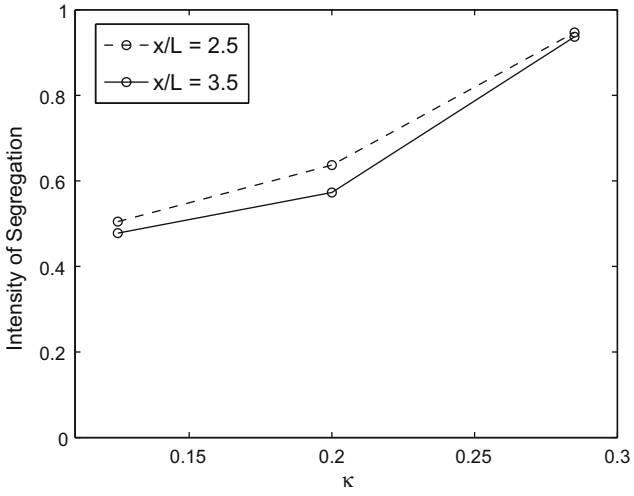

Fig. 22. The intensity of segregation against the non-dimensional channel corrugation wavelength at times when slug centroid, $x/L = 2.5$ and $x/L = 3.5$. The mixing increases as κ decreases. ($Ca = 0.005, Re = 0.64, \lambda = 0.014, \Lambda = 2.0, \eta = 0.75$, $r = 0.1$, grid: 1728×64.)

effects of channel corrugation wavelength on the quality of mixing in Figs. 20–22. The computations are performed for the corrugation wavelengths of $\kappa = 0.125, 0.2$ and 0.285 while the other parameters are the same as those in the base case. It is clear from these figures that the best mixing is achieved for the base case, i.e., $\kappa = 0.125$ and mixing dramatically decreases when κ is increased. Note that the dependence of the quality of mixing on the channel curvature is recently investigated experimentally by Fries and von Rohr (2009) using five different micromixers with a fixed length but varying channel width and bend curvature. They also observed enhanced mixing as the bend turning radius decreases, which corresponds to a decreasing κ for our setup.

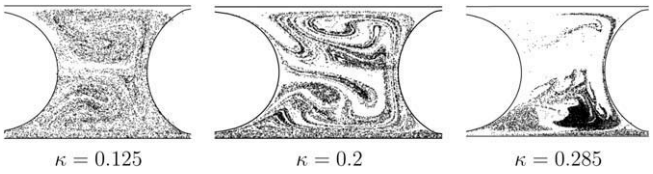

Fig. 20. The mixing patterns at the exit of the channel as a function of the non-dimensional corrugation wavelength of the channel, κ. ($Ca = 0.005, Re = 0.64$, $\lambda = 0.014, \Lambda = 2.0, \eta = 0.75, r = 0.1$, grid: 1728×64.)

5. Conclusions

The chaotic mixing in the liquid slugs between bubbles moving through a serpentine channel is studied computationally using the FV/FT method (Muradoglu and Kayaalp, 2006) in a two-dimensional setting. Scatter plots of tracer particles are used to visualize the mixing patterns and, following Muradoglu and Stone (2005), the entropy and intensity of segregation measures are used to quantify the quality of mixing. Both of the mixing measures are found to be consistent with each other and with the visual evaluations of mixing for all the cases presented. It is observed that a chaotic mixing occurs due to recirculation within the liquid slug as it moves through a winding channel. The effects of the relevant non-dimensional parameters on mixing are examined. It has been found that the chaotic advection occurs as long as segmentation is achieved. In this regard, the capillary number influences mixing significantly as segmentation occurs only when the capillary

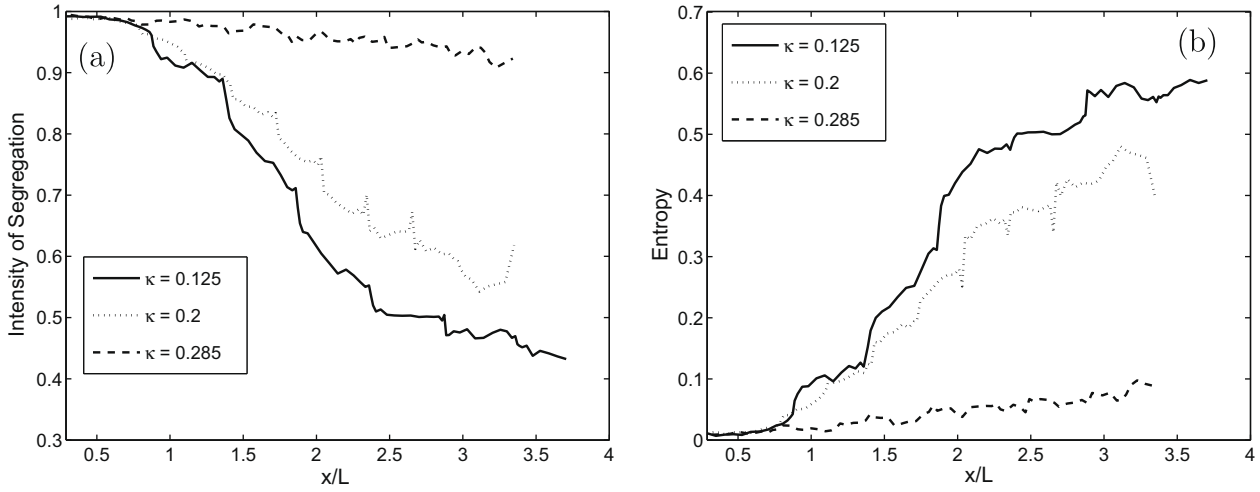

Fig. 21. Effect of the channel geometry on mixing. (a) Intensity of segregation (b) entropy. ($Ca = 0.005, Re = 0.64, \lambda = 0.014, \Lambda = 2.0, \eta = 0.75, r = 0.1$, grid: 1728×64.)

number is sufficiently small, i.e., $Ca \leqslant 0.01$ for the present case. Once segmentation occurs, a further decrease in capillary number does not affect the quality of mixing significantly. The relative size of the bubble influences the mixing in a similar fashion. Segmentation and thus the chaotic mixing occurs within the liquid slug when the bubble size is larger than the width of the channel, i.e., when $\Lambda \geqslant 1$. The viscosity ratio is found not to have any significant influence on the quality of mixing when $\lambda \leqslant 1$, which is in contrast with the mixing in a droplet moving through a serpentine channel (Muradoglu and Stone, 2005) where the viscosity ratio plays a primary role on the mixing. The mixing is found to weakly depend on the Reynolds number in the range between $Re = 0.64$ and $Re = 64$. The quality of mixing deteriorates slightly as the Reynolds number increases. The relative initial distance between bubbles is also found to be an important parameter influencing the quality of mixing and it is found that the best mixing occurs at about $\eta = 0.75$. Another important geometric parameter is the corrugation wavelength of the mixing section of the channel. It is found that the quality of mixing is influenced significantly with the non-dimensional corrugation wavelength and the larger the corrugation wavelength the better the quality of mixing in the range of $0.125 \leqslant \kappa \leqslant 0.285$.

Finally, we note that an important factor influencing the segmentation and quality of mixing within the liquid slug is the axial dispersion due to leakage through the liquid film between bubble and the channel wall. Muradoglu et al. (2007) showed that there is no axial dispersion in the absence of the molecular diffusion when the channel is straight. However, our numerical simulations indicate that there is significant axial dispersion in the curved channel even in the absence of molecular diffusion due to the fact that the liquid film thickness depends on the channel curvature (Muradoglu and Stone, 2007) and changes periodically as the bubbles move through a serpentine channel. This issue is a subject of our current study and will be reported separately in the future.

Acknowledgements

The present work is supported by the Scientific and Technical Research Council of Turkey (TUBITAK) under Grant Nos. 105M043 and 108M238. We thank Prof. H.A. Stone for helpful conversations in the early stage of this work.

References

Ahn, Y.C., Jung, W., Chen, Z., 2008. Optical sectioning for microfluidics: secondary flow and mixing in a meandering microchannel. Lab Chip 8, 125–133.
Aref, H., 1984. Stirring by chaotic advection. J. Fluid Mech. 143, 1–21.
Bajer, K., Moffat, H.K., 1990. On a class of steady confined Stokes flows with chaotic streamlines. J. Fluid Mech. 212, 337–363.
Bretherton, F., 1961. The motion of long bubbles in tubes. J. Fluid Mech. 10, 166–188.
Caughey, D.A., 2001. Implicit multigrid computation of unsteady flows past cylinders of square cross-section. Comput. Fluids 30, 939–960.
El-Ali, J., Gaudet, S., Guenther, A., Sorger, P.K., Jensen, K.F., 2005. Cell stimulus and lysis in a microfluidic device with segmented gas–liquid flow. Anal. Chem. 77, 3629–3636.
Fries, D.M., von Rohr, P.R., 2009. Liquid mixing in gas–liquid two-phase flow by meandering microchannels. Chem. Eng. Sci. 64, 1326–1335.
Garstecki, P., Fischbach, M.A., Whitesides, G.M., 2005. Design for mixing using bubbles in branched microfluidic channels. Appl. Phys. Lett. 86, 244108.
Garstecki, P., Fuerstman, M.J., Fischbach, M.A., Sia, S.K., Whitesides, G.M., 2006. Mixing with bubbles: a practical technology for use with portable microfluidic devices. Lab Chip 6, 207–212.
Gaskell, P.H., Gurcan, F., Savage, M.D., Thompson, H.M., 1998. Stokes flow in a double-lid-driven cavity with free surface side walls. Proc. Inst. Mech. Eng. 212, 387–403.
Guenther, A., Khan, S.A., Thalman, M., Trachsel, F., Jensen, K.F., 2004. Transport and reaction in microscale segmented gas–liquid flow. Lab Chip 4, 278–286.
Gunther, A., Jhunjhunwala, M., Thalmann, M., Schmidt, M.A., Jensen, K.F., 2005. Micromixing of miscible liquids in segmented gas–liquid flow. Langmuir 21, 1547–1555.
Kang, T.G., Hulsen, M.A., Anderson, P.D., den Toonder, J.M.J., Meijer, H.E.H., 2007. Chaotic advection using passive and externally actuated particles in a serpentine flow. Chem. Eng. Sci. 62, 6677–6686.
Khan, S.A., Guenther, A., Schimidt, M.A., Jensen, K.F., 2004. Microfluidic synthesis of colloidal silica. Langmuir 20, 8604–8611.
Krasnopolskaya, T.S., Meleshko, V.V., Peters, G.W.M., Meijer, H.E.H., 1999. Mixing in Stokes flow in an annular wedge cavity. Eur. J. Mech. B/Fluids 18, 793–822.
Kroujiline, D., Stone, H.A., 1999. Chaotic streamlines in steady bounded three-dimensional Stokes flows. Physica D 130, 105–132.
Meleshko, V.V., Malyuga, V.S., Gomilko, A.M., 2000. Steady Stokes flow in a finite cylinder. Proc. R. Soc. Lond. A 456, 1741–1758.
Muradoglu, M., Gokaltun, S., 2004. Implicit multigrid computations buoyant drops through sinusoidal constrictions. J. Appl. Mech. Trans. ASME 71, 857–865.
Muradoglu, M., Stone, H.A., 2005. Mixing in a drop moving through a serpentine channel: a computational study. Phys. Fluids 17, 073305.
Muradoglu, M., Kayaalp, A.D., 2006. An auxiliary grid method for computations of multiphase flows in complex geometries. J. Comput. Phys. 214, 858–877.
Muradoglu, M., Gunther, A., Stone, H.A., 2007. A computational study of axial dispersion in segmented gas–liquid flow. Phys. Fluids 19, 072109.
Muradoglu, M., Stone, H.A., 2007. Motion of large bubbles in curved channels. J. Fluid Mech. 570, 455–466.
Ottino, J.M., 1989. The Kinematics of Mixing. Cambridge University Press, Cambridge, UK.
Shui, L., Eijkel, J.C.T., van den Berg, A., 2007. Multiphase flows in microfluidic systems – control and applications of droplets and interfaces. Adv. Colloid Interface Sci. 133, 35–49.
Song, H., Tice, J.D., Ismagilov, R.F., 2003. A microfluidic system for controlling reaction networks in time. Angew. Chem. Int. Ed. 42, 768–772.
Stone, H.A., Nadim, A., Strogatz, S.H., 1991. Chaotic streamline inside drops immersed in steady Stokes flows. J. Fluid Mech. 232, 629–646.
Stone, H.A., Stroock, A.D., Ajdari, A., 2004. Engineering flows in small devices: microfluidics toward a lab-on-a-chip. Annu. Rev. Fluid Mech. 36, 381–411.
Stone, Z.B., Stone, H.A., 2005. Imaging and quantifying mixing in a model droplet micromixer. Phys. Fluids 17, 063103.
Tryggvason, G., Bunner, B., Esmaeeli, A., Juric, D., Al-Rawahi, N., Tauber, W., Han, J., Nas, S., Jan, Y.-J., 2001. A front-tracking method for the computations of multiphase flow. J. Comput. Phys. 169, 708–759.
Unverdi, S.O., Tryggvason, G., 1992. A front-tracking method for viscous, incompressible flows. J. Comput. Phys. 100, 25–37.
Yen, B.K.H., Guenther, A., Schmidt, M.A., Jensen, K.F., Bawendi, M.G., 2005. A microfabricated gas–liquid segmented flow reactor for high temperature synthesis: the cas of CdSe quantum dots. Angew. Chem. Int. Ed. 44, 2–6.
Yu, Z., Hemminger, O., Fan, L.S., 2007. Experiment and lattice Boltzmann simulation of two-phase gas–liquid flows in microchannels. Chem. Eng. Sci. 62, 7172–7183.